

Chapter 2

Thermal Regimes and Effects

Pyrometamorphism related to intrusion of mafic magma and the burning of organic material is expected to result in anisotropic thermal expansion and associated positive volume changes in contact rocks due to reaction and melting of the mineral phases. Columnar jointing, cracking and dilation are typical of the structures developed. Temperature variation can be extreme with thermal gradients of several hundred degrees developed over a few meters or even tens of centimeters, particularly in the case of combustion, and lightning strike metamorphism where extreme temperature gradients occur over a few millimeters.

2.1 Igneous Pyrometamorphism

2.1.1 *Aureoles*

Pyrometamorphism affects rock that is in contact with intrusion of typically mafic-intermediate magmas. Evidence of pyrometamorphosed metasediment, metabasite, and granitic host rocks intruded by shallow basaltic and andesitic plugs, sills and dykes has been reported from many localities, commonly with the development of buchites in the case of psammitic-pelitic protoliths. Mineral reconstitution is largely restricted to within about 0.5 m of the igneous contacts, but in some cases the thermal effects and their resultant structures such as columnar jointing are locally developed up to 50 m from the contact.

The generation of very high temperatures, sometimes approaching 1200°C, in contact aureoles results in steep thermal gradients and has been ascribed to flow of magma through conduits that represent feeders of lava flows, turbulent magma flow (e.g. in sills), convective circulation in larger magma bodies or relatively short filling times in the order of <100 years, geologically “instantaneous” (a few days) intrusion in the case of smaller bodies, and both convective and conductive heat transfer via water through the contact rocks. While various temperature profiles constructed normal to the igneous contacts have been attempted using appropriate mineral equilibria (see below), estimation of the timing of the pyrometamorphic event is more difficult, although the use of Ar and element diffusion profiles and modeled changes in thermal profiles with time have been made (e.g. Wartho et al. 2001).

The efficiency of heat transfer of magma through a conduit is critically dependent on the magma flow regime. Turbulent flow can dramatically increase temperatures in contact country rock to approach that of the magma (Huppert and Sparks 1985) resulting in fusion and the development of a wide aureole. Rocks containing substantial modal K-feldspar, Na-plagioclase, quartz and muscovite/biotite, e.g. pelite, arkose, granite-granodiorite, tend to fuse more readily than refractory lithologies such as quartzite, adjacent turbulent basaltic magma. Turbulence is commonly associated with high flow rate and reduced viscosity, particularly where the conduit acts as a feeder to lava flows. It may develop around areas of local irregularities in the wall rock, where there is a marked change in the attitude or a change in thickness of the intrusive body. In comparison, laminar flow typically results in chilling and a relatively low contact temperature of perhaps midway between that of the magma and the mean temperature of the country rock prior to intrusion (e.g. Delaney and Pollard 1982). Where heat conduction is the only mechanism of energy transport within the magma and contact rocks, the maximum temperature attained at a contact is equal to about two-thirds of the solidus temperature of the magma (Jaeger 1968, pp. 520–523). On the other hand, convection in a narrow boundary layer along a vertical contact will maintain the contact temperature at or even slightly above that of the basaltic solidus during the early stages of crystallisation (Shaw 1974).

Thermal modeling of the contact rock considering a basaltic sill of half thickness h emplaced in country rock with the same thermal conductivity, specific heat capacity and density or thermal diffusivity κ as the magma, and ignoring the latent heat of magma crystallization is detailed by Wartho et al. (2001) using three models;

1. Conductive cooling following instantaneous emplacement
2. Convection driven by heat loss into the roof rocks of the sill while the floor remains insulated following instantaneous emplacement
3. The magma/country rock contact is held at a constant temperature as in the case where prolonged turbulent flow of magma through the sill maintains the magma emplacement temperature along the contact.

The three models are illustrated in Fig. 2.1 in terms of time-temperature relationships at dimensionless temperatures (T), distances (y) and times (t) from the igneous contact. Temperature at any position in the country rock at a particular time can be found in terms of the following dimensionless variables:

Dimensionless temperature =

$$\theta = \frac{T - T_{\text{cr}}}{T_{\text{mag}} - T_{\text{cr}}}$$

Dimensionless distance =

$$Y = y/h$$

Dimensionless time =

$$\tau = \kappa t/h^2$$

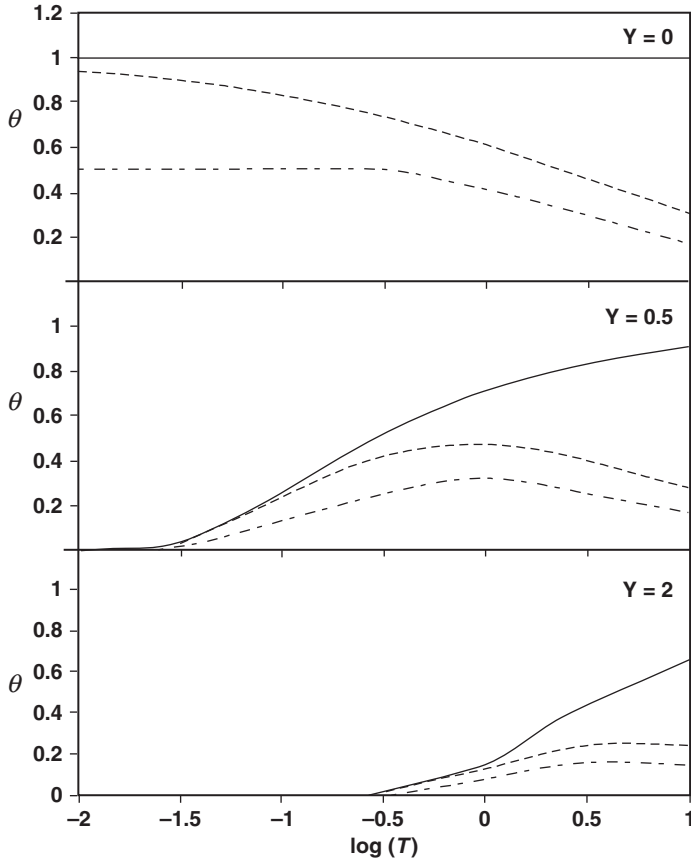


Fig. 2.1 Temperature-time relationships for three thermal models at dimensionless distances ($Y = 0, 0.5$ and 2) from the contact of the sill. *Short-long dash line* = θ_{cond} (model 1); *dashed line* = θ_{conv} (model 2); θ_{cond} (model 3) (redrawn from Fig. 1 of Wartho et al. 2001). See text

where T_{mag} = initial magma temperature and T_{cr} = initial contact rock temperature.

Following Jaeger (1964), the temperature-position-time relations for the three models are;

Conductive cooling (θ_{cond}) (model 1)

$$\theta_{\text{cond}} = 0.5 \left\{ \operatorname{erf} \left(\frac{Y+2}{2\tau^{1/2}} \right) - \operatorname{erf} \left(\frac{Y}{2\tau^{1/2}} \right) \right\}$$

Convective cooling above upper contact (θ_{conv}) (model 2)

$$\theta_{\text{conv}} = \exp \left\{ \frac{Y}{2} + \frac{\tau}{4} \right\} \left[\operatorname{erfc} \left(\frac{Y}{2\tau^{1/2}} + \frac{\tau^{1/2}}{2} \right) \right]$$

Continuous turbulent intrusion (θ_{cont}) (model 3)

$$\theta_{\text{cont}} = \operatorname{erfc}\left(\frac{Y}{2\tau^{1/2}}\right)$$

The models predict, for example, that at the contact ($Y = 0$), the temperature remains at $\theta = 1$ for as long as the magma is flowing, whereas in the conductive model, θ does not exceed 0.5. In the convective model, θ is initially 1 and then gradually decreases until reaching 0.5 at $\tau \sim 3$. At any given time the prolonged turbulent emplacement model gives the highest temperature and the conductive model the lowest temperature. Under conditions of $Y = 2$ the thermal histories are virtually indistinguishable after $\tau \sim 1$. It can also be noted that in all three models, heating will be greater above than below the sill, whereas under conditions of conductive cooling or forced flow heating will be symmetrical. Wartho et al. (2001) point out that the symmetry of thermal metamorphism and the maximum temperatures reached at given distances, especially those near the contact, should be sufficient to constrain the dominant heat transfer process.

Koritnig (1955) has calculated a number of heating curves over a period of 180 days in sandstone adjacent the Blaue Kuppe dolerite, Germany, and also heating profiles developed within 100 cm of the contact over a period of 3 days (Fig. 2.2). In both cases a constant temperature of 1200°C is maintained along the contact, implying magma flow. The curves, for example, show that temperatures of 1000°C in sandstone 0.5 m from the contact may be reached after ~20 days and after 180 days 2 m from the contact. After little more than 1 day, the temperature of sandstone 10 cm from the contact is 1000°C. The temperature-distance relations are supported by the abundance of glass present in the contact rocks which can be described as buchites. The calculated temperature curves ignore the role of the expulsion of intergranular fluid from the sandstone that is effective in transferring heat.

In Fig. 2.3, thermal profiles away from roughly circular gabbro (~50 m) and peridotite (200 m) plugs on Rhum, Scotland, are shown together with melt volume generated in their respective aureole arkose rocks (Holness 1999). The onset of melting occurs at a distance of ca. 15 m from the gabbro but only 6 m away from the peridotite, and in both cases the amount of melt increases abruptly with the beginning of melting, both reaching 75 vol.% within a few metres. Application of a simple, one-dimensional, two-stage model to both aureoles is made by Holness (1999), assuming:

1. The intrusions are vertical cylinders intruded into country rock with an initial ambient temperature of 30°C
2. 1st stage of thermal history; contact kept at constant temperature to simulate flow of magma through cylindrical conduits
3. 2nd stage of thermal history; cooling only that occurs after end of magma flow
4. Thermal diffusivity of both intrusions and country rock = $10^{-6} \text{ m}^2 \text{ s}^{-1}$ and heat capacity = $2.5 \text{ J cm}^{-3} \text{ K}^{-1}$.

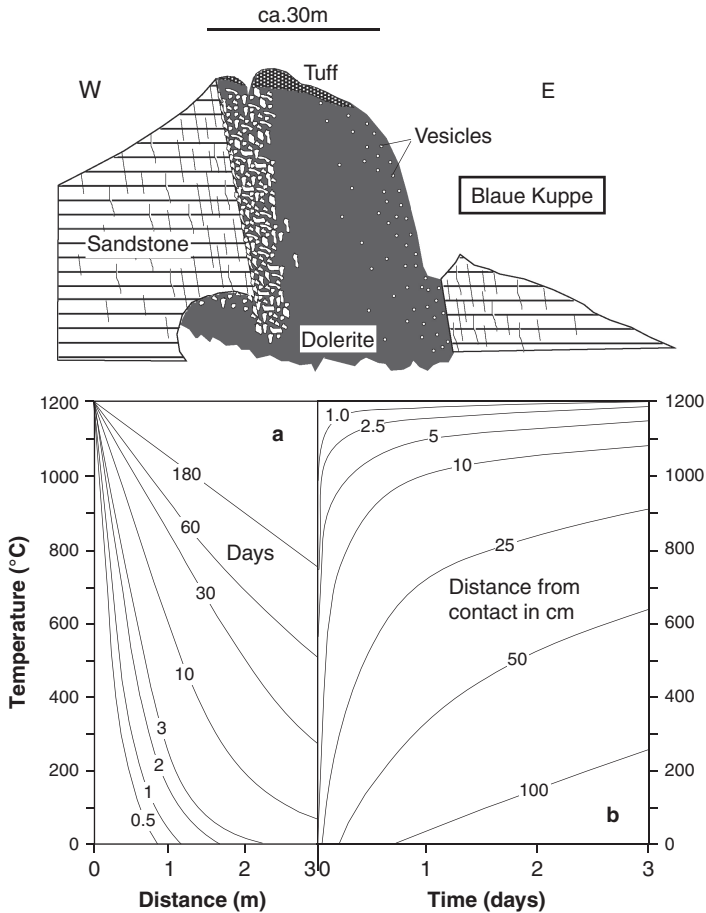


Fig. 2.2 An E-W cross section of the Blaue Kuppe dolerite, near Eschwege, Germany (redrawn from Fig. 5b of Koritnig 1955). Below: (a) Heating curves for sandstone within 3 m of the dolerite contact assuming a constant contact temperature of 1200°C over a period of 180 days; (b) Heating curves for sandstone within 100 cm of the contact over 3 days assuming a constant contact temperature of 1200°C (redrawn from Figs. 8 and 9 respectively, of Koritnig 1955)

5. The latent heat of melting of a country rock arkose of 50 wt.% quartz, 25 wt.% albite, 25 wt.% orthoclase is modeled using expressions of Burnham and Nekvasil (1986) for latent heats of fusion of end member feldspar components. The latent heat of fusion of magma can be ignored in view of the fact that the latent heat of fusion of melting of country rock has no appreciable effect on T_{\max} curves in Fig. 2.3.

The results of the thermal modeling are that for a peridotite magma temperature of 1000–1200°C, intruded as a single stage crystal-rich mush, the heating lasted

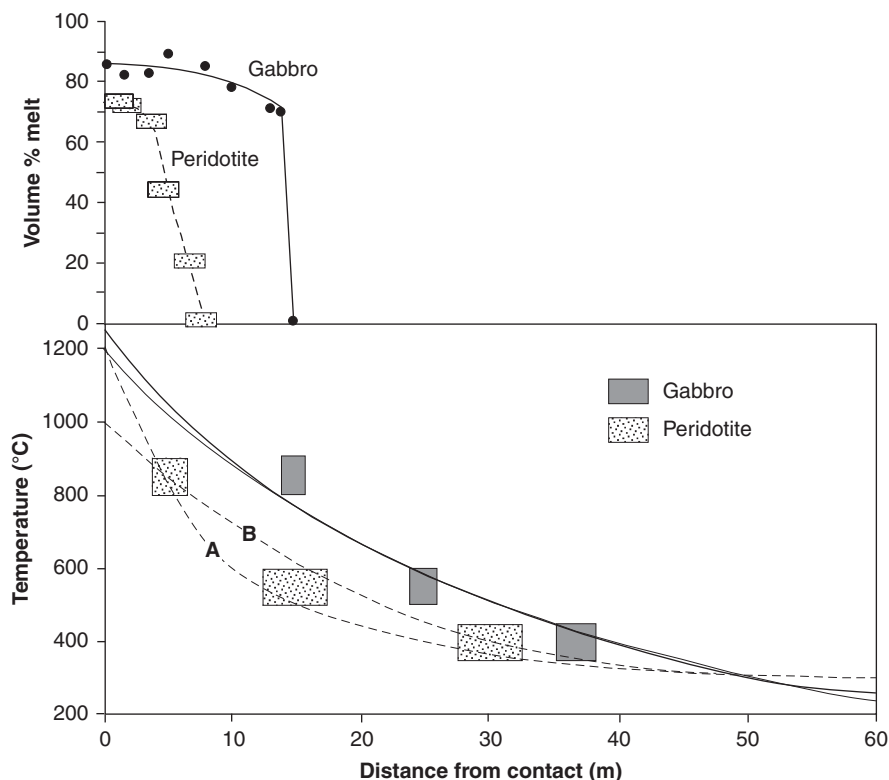


Fig. 2.3 Thermal profiles (T_{\max}) (below) and melt contents (vol.%) (above) for arkosic country rock surrounding gabbro and peridotite plugs, Mull, Scotland (redrawn from Figs. 11 and 6, respectively, of Holness 1999). See text. Uncertainty in temperature due to insufficient experimental data for melting (first appearance of melt), variable bulk Fe content relating to chlorite breakdown reaction, and uncertainty about kinetics of microcline-sanidine transition. Uncertainty in distance due to exposure and finite sample spacing. *Curve A* = magma T 1200°C, contact remains at constant T for 3 years; *curve B* = magma T 1000°C, contact remains at constant T for 10 years. *Unlabelled two curves* fitting gabbro data = magma T 1250°C, contact T remains constant for 35 years, and for magma T 1200°C, constant contact temperature for 40 years

3–10 years; for a gabbro magma temperature of 1200–1250°C, a constant contact temperature lasted 35–40 years due to magma flow through the conduit. The calculated contact temperatures also predict complete melting of the country rock within 10 m of the gabbro contact and within a few metres of the peridotite. This is not the case (Fig. 2.3), suggesting that either melting was inhibited by factors such as kinetics of the melting reactions or availability of H_2O , or the models are unrealistic close to the contacts. Within 10 m of the gabbro, the model predicts that all melt solidified within 10 years of the onset of the 2nd stage cooling. That cooling to temperatures below the solidus occurred with ca. 5 years is supported by evidence of destruction of millimetre-scale layers rich in detrital magnetite in the arkose within

10 m from the gabbro contact. From Stokes' law, the velocity at which spherical particles of radius r fall through a liquid of viscosity μ is given by

$$v = \frac{2gr^2\Delta\rho}{9\mu}$$

where g = acceleration due to gravity; $\Delta\rho$ = difference between density of solid (magnetite of 5.3 gcm^{-2}) and liquid (melt of 2.3 gcm^{-1}); melt viscosity (μ) = 10^6 – 10^7 poise. A magnetite crystal of 0.1 mm diameter will drop by 1 cm in 170–1700 days thus obliterating the fine-scale layering.

2.1.2 Xenoliths

The preservation of pyrometamorphosed suites of xenoliths characterised by different mineral assemblages within individual magmatic bodies implies mechanical disintegration of various source lithologies of a deeper contact zone. In areas where igneous contacts are irregular, mechanical erosion of wall rock of suitable composition may occur leading to concentrations of xenoliths such as observed in thin (up to 6 m wide) basic sheets of the Ross of Mull peninsula, Scotland (e.g. Killie et al. 1986; Fig. 2 of Holness and Watt 2001), or along the contact of a steeply dipping pipe-like body such as Blaue Kuppe, Germany (Fig. 2.2). Xenolith population sizes are typically small, a few centimetres to several tens of centimeters in diameter, although occasional rafts several meters across and length (rarely with outcrop dimensions of several hundred meters by several kilometers) also occur. In more homogeneous lithologies such as quartzite and sandstone, the resultant xenoliths tend to be blocky and are often larger compared with those of rocks that are layered on a scale of a few millimeters to centimeters, e.g. as in schist. Very large blocks, tens to a hundred meters or more in diameter, usually of coarsely crystalline rock, e.g. granite or homogeneous sandstone, are usually found close to their wall rock source.

Once rock temperatures attain values where melting (usually along quartz-feldspar contacts) occurs, the rigidity and mechanical integrity of the rock becomes significantly reduced and in wall rocks unstable portions tend to be dislodged and entrained within the magma (Fig. 2.4). Further disaggregation, for example of mica-rich and quartz/feldspar-rich parts (greater than a few mm thick) in schist blocks engulfed in magma, is generally the rule with each part undergoing different paths and rates of bulk melting and recrystallisation. Partially melted/reconstituted mica-rich layers tend to form rafts whereas interlayered quartz-feldspar rich layers may temporarily remain as scattered clots of partially melted (rounded and resorbed) grains of quartz and sometimes feldspar in a siliceous melt (Fig. 2.5).

Lovering (1938) has calculated that the temperature in the core of a 2 m thick xenolith of marble heated by conduction would approach that of the surrounding magma within a few weeks implying that the formation temperature of pyrometamorphic mineral assemblages in the xenolith can be equal to the magma

Fig. 2.4 Schematic diagram showing formation and evolution of xenoliths in turbulent basaltic magma intruding a layered meta-sandstone–siltstone sequence (redrawn and modified from Fig. 15 of Preston et al. 1999)

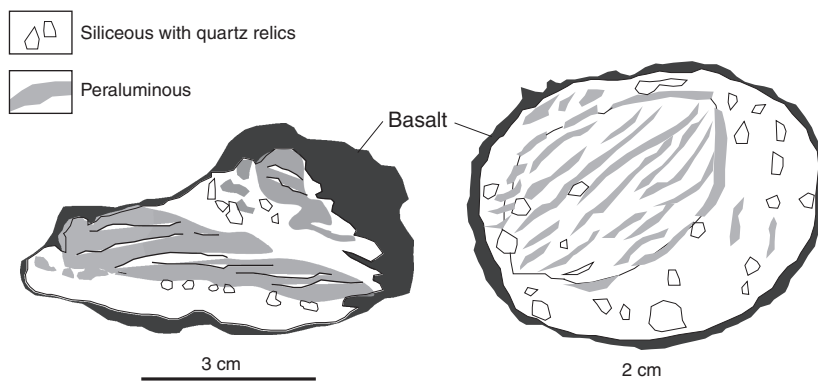
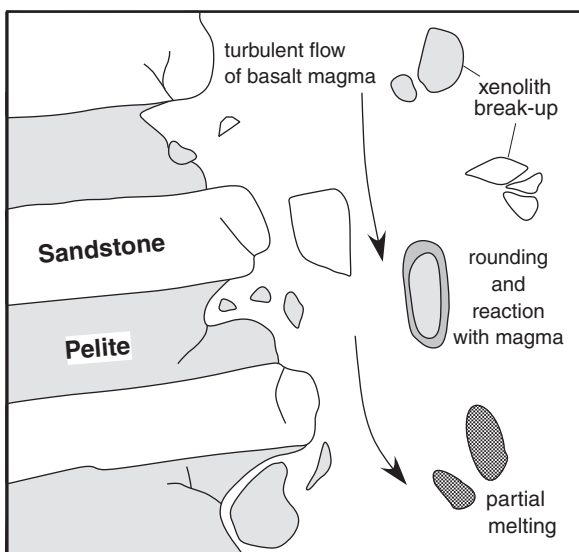


Fig. 2.5 Sketches of two partially melted xenoliths occurring in Recent hawaiites from Mt. Etna, Italy (redrawn from Fig. 11 of Michaud 1995). *Siliceous parts* contain cristobalite, tridymite in alkali-rich acidic glass. Quartz, zircon, apatite and titanite remain as relics. *Peraluminous parts* contain cordierite, spinel, Ca-plagioclase, magnetite-ilmenite and rutile in peraluminous (often K or K + Fe-rich) glass

temperature. An analysis of the heating and partial melting of a xenolith during cooling of a mafic magma is given in the schematic diagram shown in Fig. 2.6 after Wyllie (1961). The diagram shows a lag time between the heating of the xenolith (T_1) and formation of melt (t_2) at which time the temperature of the xenolith is increased to T_2 with an equilibrium melt for this temperature forming at t_4 . At t_4 the temperature of the xenolith has increased to that of the cooling magma. By t_5 both magma and xenolith have cooled to T_3 . While the magma cooled from T_4 to T_3 , the

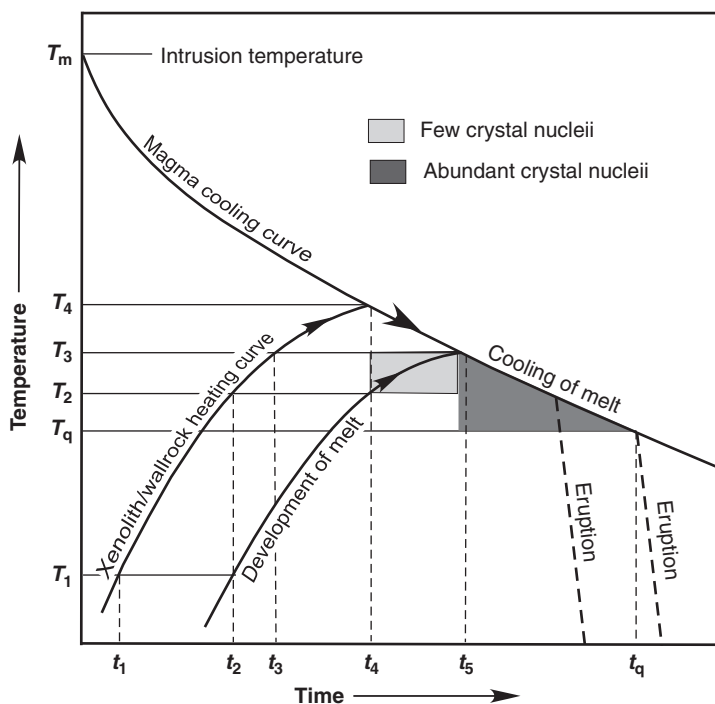


Fig. 2.6 Schematic diagram showing relationships between cooling curve of mafic magma, heating curve of a xenolith, and curve of equilibrium melt formation in the xenolith. *Horizontal lines* between xenolith heating and melt formation curves represent the time-lag between the two (redrawn and modified from Fig. 4 of Wyllie 1961). Additional T - t regions of formation of few and abundant crystal nuclei in the melt are also shown together with possible quenching on eruption trajectories. See text

xenolith continued to melt and reached its maximum state of fusion at T_3 . After t_5 , magma and melt within the xenolith cool together with crystallization of minerals from the melt and with remaining melt quenched at t_q .

Because heating times during pyrometamorphism are fast and relatively short, the rate of crystal nucleation will also lag behind the change in temperature. Peak metamorphic temperatures are unlikely to be maintained for very long before cooling commences (T_3 at t_5) and as the rate of cooling is significantly less than the rate of heating, most crystallization will probably occur during the period of cooling under nearly isothermal conditions as shown and cease with quenching on eruption.

Thermal modeling of a partially melted xenolith of granite in a cooling stock of trachyandesite and of granite surrounding the plug is analysed by Tommasini and Davies (1997). Dimensions and thermal conditions for the modeling are:

Plug: Diameter = 50 m, intrusion temperature = 1100°C , heat of crystallisation = 400 kJ/kg (effective thermal diffusivity κ of trachyandesite $9 \cdot 10^{-7}$ – $2.6 \cdot 10^{-7} \text{ m}^2\text{s}^{-1}$)

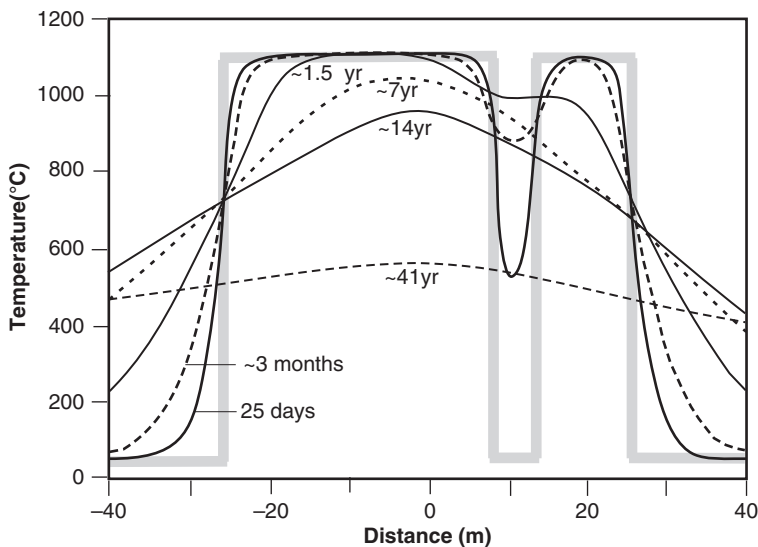


Fig. 2.7 Temperature-distance-time profiles of a cooling 50 m diameter trachyandesite plug intruding granite and containing a 4 m wide block of granite (redrawn from Fig. 4 of Tommasini and Davies 1997). See text

Granite xenolith: Width = 4 m; beginning of melting = 850°C at $P_{load} < 500$ bars; heat of fusion = 300 kJ/kg (effective thermal diffusivity κ of granite $1 \cdot 10^{-6}$ – $4.4 \cdot 10^{-7}$ m²s⁻¹).

Country rock granite: Maximum temperature = 50°C at time of intrusion.

The resulting temperature-distance-time profiles shown in Fig. 2.7 indicate that the granite xenolith reaches solidus temperature within ~3 months and attains a maximum temperature of ~1000°C after ca. 1.5 years. For melting to occur in the granite country rock, the initial intrusion temperature of the trachyandesite of 1100°C would need to be maintained by a constant flow of magma. The time required to reach the granite solidus temperature obtained from

$$T_i = T_{\text{magma}} \left[1 - \operatorname{erf} \left(\frac{x_i}{\sqrt{4\kappa t}} \right) \right]$$

where T_{magma} remains constant at the contact ($x_i = 0$ m); T_i = country rock temperature at distance x_i from the contact; κ = thermal diffusivity of the granite; t = time lapsed since intrusion, indicates that after 20 days of continuous flow the temperature is >850°C (~ temperature of biotite melting) 0.5 m from the contact.

A final example illustrates temperatures generated in different shaped metabasaltic xenoliths in basaltic magma (Brandriss et al. 1996). Modeled temperature-time after stopping profiles are shown in Fig. 2.8 for conductive heating of a 4 m diameter sphere and a 4 m thick infinite slab with an initial temperature of 400°C, assuming a constant temperature of 1050°C for the magma, and a thermal diffusivity of 0.005 cm²/s for xenoliths and magma. For the spherical xenolith, the

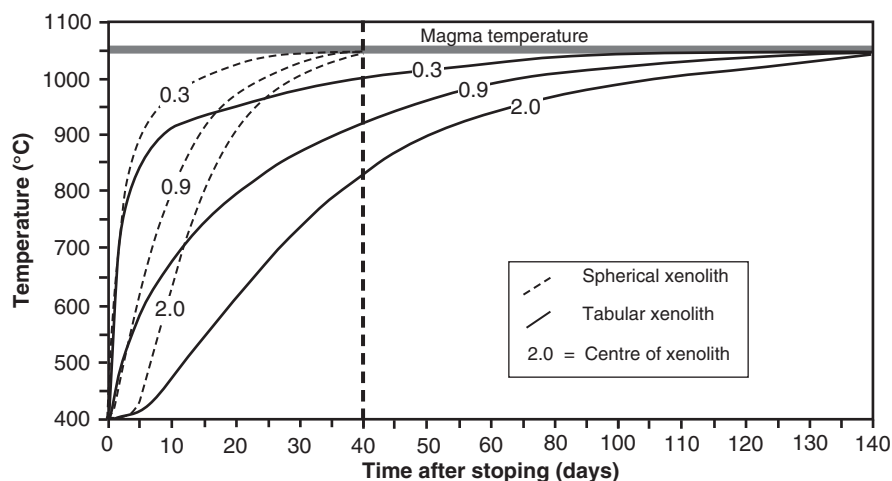


Fig. 2.8 Modelled profiles for conductive heating of a spherical xenolith 4 m in diameter (*dashed curves*) and a 4 m thick tabular xenolith (*solid curves*). Numbers on curves = distances (m) from xenolith-basalt contact (redrawn from Fig. 21 of Brandriss et al. 1996)

centre reaches 1000°C within a few weeks whereas it takes a few months for the same temperature to be reached in the central part of the tabular xenolith.

2.2 Combustion Pyrometamorphism

Baked and fused rocks developed on various scales resulting from the combustion of organic and bituminous matter, coal, oil or gas in near-surface sediments are examples of this type of pyrometamorphism where thermal energy is provided through burning. Ground magnetic and aeromagnetic surveys across areas of such combustion metamorphism indicate high anomalies in the range of several thousands of gammas (e.g. Cisowski and Fuller 1987). Temperatures attained during burning range from ~400°C to possibly as high as ~1600°C resulting in a large variety of pyrometamorphic rock products, often on the scale of a single outcrop, from thermally altered but unmelted rocks, termed *burnt rocks* or *baked rocks*, to those that are partly fused, termed *clinker*, or those that are totally melted, termed *paralava* or *slag*, as described in Chap. 1.

2.2.1 The Burning Process

The agent of combustion pyrometamorphism is heat created by oxidation of organic matter and, in many cases associated sulphides (typically pyrite), through access of atmospheric oxygen into a rock sequence by way of joints, cracks and faults, or due to exposure by slumping. Heating occurs by way of the low temperature of oxidation combined with absorption of moisture. Because of its diverse composition

and heterogeneous nature, oxidation of carbon, such as in coal, is a complex process, but a simplified exothermic reaction can be expressed as:

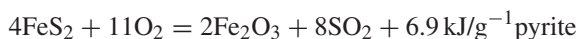


with the rate of reaction doubling for every increase of 10°C (Speight 1983). Normally the generated heat is carried away by circulation of air, but where it cannot escape, the temperature of the coal is raised to its “threshold temperature” of somewhere between 80 and 120°C where a steady reaction resulting in the production of gases such as CO₂, CO and H₂O occurs. As the temperature continues to rise to somewhere between 230 and 280°C, the reaction becomes rapid and strongly exothermic and spontaneous combustion occurs when the coal reaches its ignition point. While changes in moisture and oxidation can explain most spontaneously-generated heat in coal, there are several other important contributors to its pyrophoricity such as:

Rank. As coal rank decreases, the tendency for self-heating increases. Sub-bituminous coals tend to have a higher percentage of reactive macerals such as vitrinite and exinite that increase the tendency of coal to self heat.

Particle size. There is an inverse relationship between particle size and spontaneous combustion; the smaller the particle size the greater surface area available on which oxidation can take place,

Pyrite content. The presence of pyrite and marcasite (usually in concentrations > 2 vol.%) may accelerate spontaneous heating by reaction with oxygen according to the equation



Both pyrite and marcasite swell upon heating. This causes the surrounding coal to disintegrate resulting in a reduction of the particle size involved in oxidation reactions.

Temperature. The higher the temperature, the faster coal reacts with oxygen.

Air flow. The flow of air provides the oxygen necessary for oxidation to occur and at the same time can also remove heat as it is generated.

Geological/environmental factors. Sedimentary rocks which enclose coal seams or organic matter are poor conductors of heat. Faults and fractures in the rocks allow the influx of water and oxygen enhancing oxidation and heating. Areas of extensive combustion metamorphism are typically associated with anticlinal or rift structures where fracturing allows the access of oxygen. Drying and microbial decomposition of subsurface organic material will also result in heat production to the point of self ignition.

2.2.1.1 Coal Seams

The generally applicable nature of the burning process and the structures produced from the combustion of coal seams is discussed by Sigsby (1966) and Heffern and Coates (2004) in relation to burning lignite seams in North Dakota and high-volatile

Fig. 2.9 Map showing extent (5 ha) of an active coal-seam fire and fissures extending beneath a hill side (contour pattern indicated by *thin dashed lines*) fronted by a river (Tongue River), Acme underground coal mine, Wyoming, Powder River Basin, USA. In this case, the river and tributary streams shown have exposed the coal-seam resulting in oxidation and combustion (redrawn from Fig. 5 of Heffern and Coates 2004)

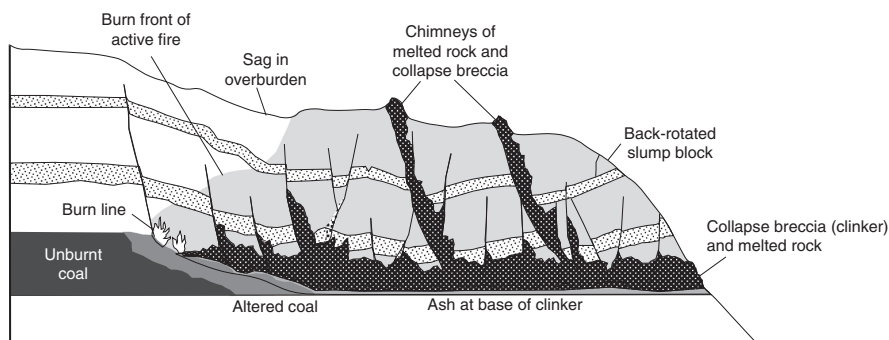
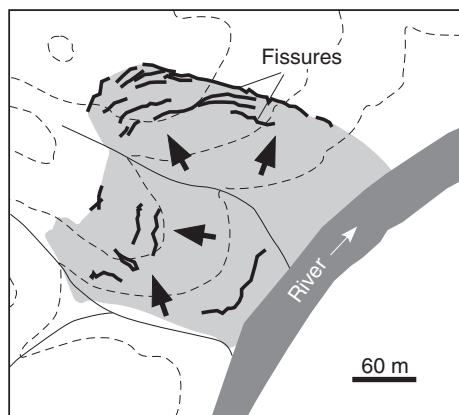


Fig. 2.10 Cross-section of a burning coal seam progressing beneath a collapsing hillside (redrawn from Fig. 7 of Heffern and Coates 2004)

sub-bituminous coal in the Powder River basin of Wyoming and Montana, respectively. Whatever the cause (oxidation on exposure to the atmosphere, lightning, prairie fire, etc), combustion always starts at the surface, often where exposures are made by rapidly cutting streams (Fig. 2.9). In the initial stages when fire spreads laterally along exposed lignite or coal and back into the outcrop, the overlying rocks progressively subside into the burned-out void (Fig. 2.10) to form a breccia or, where there are clay horizons a crumpling of slumped, coherent strata occurs. Rogers (1917) concluded that in general, where there is a cover of more than 15–30 m, and where the coal seam is horizontal, burning does not extend more than 60–90 m back from the outcrop. Field observations indicate that thin seams appear to be less commonly burnt than thick ones and seams of impure coal burn less commonly than those of cleaner coal.

Fracturing of the overburden overlying the burning and burnt-out coal seam allows air to enter and gases to escape allowing the burning to continue. If the air supply is unrestricted, strongly oxidizing conditions causes reddening of the roof rocks for a few centimeters. The fire may smolder for long periods, but can sometimes flare into an inferno producing temperatures high enough to melt rocks.

The fire will naturally extinguish itself if the overburden is thick and fractures from collapse fail to reach the surface, or where the fire has burned down to the level of the water table in the coal. Reduced conditions coupled with conservation of heat produced by a thicker, more competent overburden causes partial distillation of the coal to form coke and resultant production of CO and H₂O which disassociates allowing the formation of more CO in addition to H₂. Along with SO₄ from the breakdown of gypsum and pyrite in the coal, these gases move upward through cracks and fractures in the roof rocks, transmitting heat by contact that can cause the wall rocks to melt. The gases also tend to cause reduction of hydrous iron oxides to ferrous compounds in the melted rock and to magnetite, as the gases tend to lose their reducing capacity in higher zones. With continued upward migration, H₂ and CO oxidize to H₂O and CO₂ and still retain sufficient heat to cause baking and resultant oxidation of iron compounds to produce the typical reddening effect commonly observed.

Sedimentary rocks overlying the burning coal seam are thus subjected to a sequence of changes in time and space. The rocks are first hardened and yellowed by oxidation of iron present as hematite or Fe-hydroxide. With continued heating, the yellowish colours change to darker, more intense hues of orange and red in response to variations in temperature and oxygen supply that affect areas ranging from centimeters to meters in diameter (horizontally and vertically). At higher temperatures the rocks become sintered and recrystallised to produce a ceramic texture. Areas subjected to the highest temperatures, e.g. fissures and tabular chimneys of welded breccias, typically contain black, green and grey clinker and paralava “cement” (Fig. 2.12) indicating a reducing environment where iron is present as newly-formed magnetite or even metallic Fe. This paralava melt may flow into the fractures and in combination with collapsed rock fragments, clog the opening to produce a chimney assemblage and divert gases into other fractures. With erosion, these chimneys remain as remnants of hard, fused rock masses projecting through partly baked rocks (Figs. 2.11 and 2.12; see also Plate 1A of Rogers 1917). From the coal itself, combustion produces coal ash, typically a mixture of the non-combustible products such as quartz, feldspar, clays (largely kaolinite), illite, pyrite and carbonates such as calcite, ankerite and siderite, that melt from the heat of combustion to produce “pools” of paralava or slag. Clay within a meter or so of the base burnt coal seam ash may be fused to form a porcellanite clinker.

The behavior of coal fires is a function of a complex interaction between geo-mechanical effects, overburden permeability and natural convection flow of oxygen and heat flow. Two-D modeling of the interaction of underground coal fires and their roof rocks has been made by Wolf and Bruining (2007). An example of a coal fire at a depth of 40 m associated with subsidence/compaction of the overburden is shown with respect to temperature distribution and O₂-concentration distribution with convection in Fig. 2.13, and could relate to the section shown in Fig. 2.10. The area of the most intense pyrometamorphism involving melting of sedimentary rocks, coal ash and char relics is restricted to a very small area at the burning coal face and the base of active vents/faults where temperatures are > 1100°C (Fig. 2.13). Hot gases and heat from the burning zone move upward through the overburden creating areas of baked and melted rock in the wall rocks as described above.

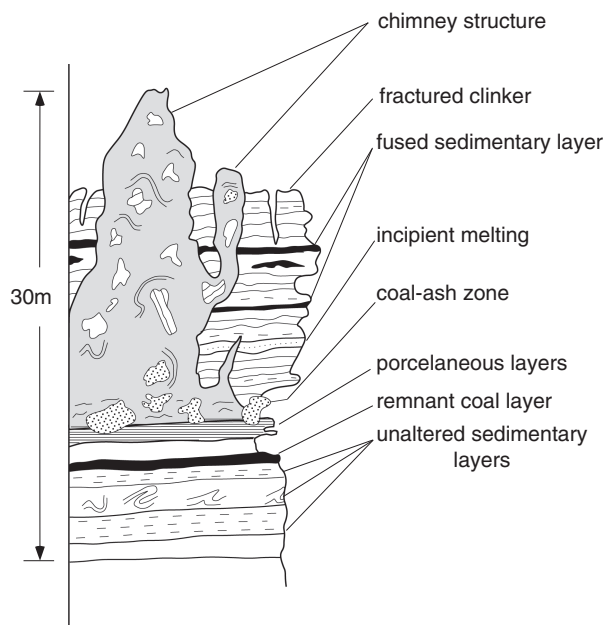
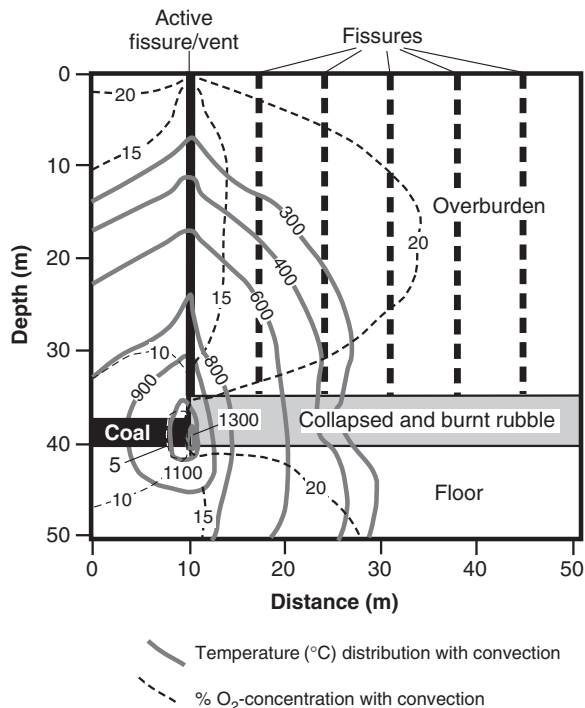


Fig. 2.11 Anatomy of a chimney structure, an erosion remnant from burning of a coal seam, consisting of black and vesiculated paralava containing clasts of clinker. The coal-ash zone is composed of glassy, vesicular paralava (redrawn from Fig. 2 of Cosca et al. 1989)



Fig. 2.12 Photos showing a clinker breccia-filled chimney structure (*left*) with the white to cream-coloured clinker breccia cemented by *dark grey-black* paralava (*right*), Kuznetsk coal basin, Siberia (photos by Ella Sokol)

Fig. 2.13 Diagram showing modelled temperature and O₂-concentration distribution with convection associated with a burning coal seam at 40 m depth (redrawn and modified from Fig. 7 of Wolf and Bruining 2007, who provide details of modelling parameters used)



An interesting example of pyrometamorphic cap rocks resulting from coal fires of Pliocene–Holocene age are recognized in NW China below river terraces (Zhang et al. 2004) (Fig. 2.14). The burnt rocks are between 100 and 150 m thick and characterised by reddish colour, millimeter-sized hexagonal columnar jointing, vesicular glassy rocks with microflow structure, porcellanitized kaolin, roof collapse and resultant brecciation, and with the coal layer reduced to an ash layer only a few centimeters thick typically rich in gypsum. Thermomagnetic analysis of burnt rock indicates the presence of trace amounts of metallic iron implying minimum temperatures of 770°C for the pyrometamorphism. Exposure of the coal and concomitant spontaneous combustion appears to be an interglacial phenomenon associated with uplift since the Pliocene when river downcutting and terrace formation occurred resulting in exposure of the coal to oxidation and resultant combustion.

2.2.1.2 Carbonaceous Sediments

For the heating and combustion of carbonaceous sediments, the situation is somewhat different and a good analysis is provided by Matthews and Bustin (1984) from variably weathered Cretaceous mudstones in the Smoking Hills area of Canadian Arctic coast (Fig. 2.15). Perhaps the earliest written report of pyrometamorphism of carbonaceous sediments in action at this locality was when smoke and sulphurous

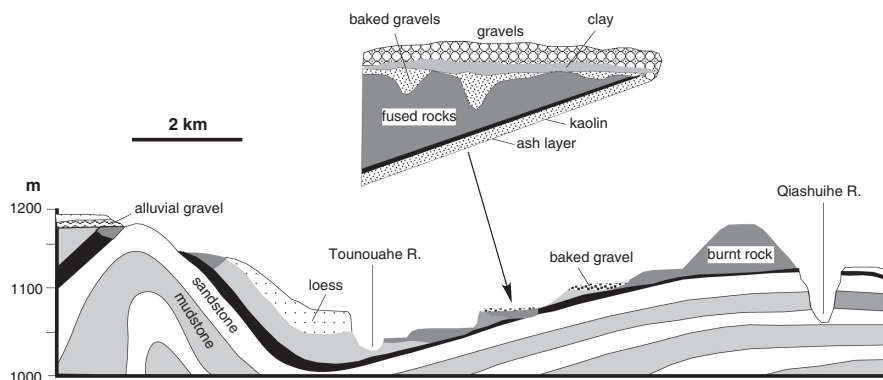


Fig. 2.14 Section centred on the Toutunhe River terrace sequence, NW China, showing occurrences of burnt rocks and a burnt rock profile (redrawn from Figs. 2 and 3 of Zhang et al. 2004). Several age groupings of combustion are identified: Pliocene-Early Quaternary at 200 m above present day flood plain; Middle Pleistocene at >90 m; Late Pleistocene at 90–70 m; Holocene; current burning sites

fumes were seen in 1826 issuing from what has since been termed the *Smoking Hills* bordering Franklin Bay, Arctic Inuvik Province of Canada, during the second over-land expedition of John Franklin and John Richardson in 1825–1827. Richardson (1851) records at “at Cape Bathurst (northern end of Franklin Bay). . . , bituminous shale is exposed in many places, and in my visit there in 1826 was in a state of ignition; and the clays which had been thus exposed to the heat were baked and vitrified, so that the spot resembled an old brick-field”. The Late Cretaceous bituminous shale with thin seams of jarosite is still burning although rarely are temperatures high enough to produce fused and vesicular clinker or paralava (Matthews and Bustin 1984). According to Yorath et al. (1969, 1975), an exposure may be quiescent 1 day, and the next it can be extremely hot producing noxious SO_4 fumes. Where the formation is burning or has been burnt, the shales are coloured bright yellow, orange, maroon and red. The red material consists of earthy hematite and at a number of localities large crystals of gypsum are scattered over burnt shale outcrops. Early geological explorations of British Columbia and the western Northwestern Territories also record localities of superficial burning (smoking) at sites of hot sulphurous gas emission, termed *bocannes*, in certain shales resulting in baking and reddening or bleaching (Crickmay 1967). As at Smoking Hills, extinct bocannes are marked by similarly coloured rocks but without smoke.

Matthews and Bustin (1984) have determined that the bocannes at Smoking Hills are fuelled by oxidation of fine grained, framboidal pyrite and/or organic matter (vitrinite and alginite) and that they are restricted to areas of glacially (?) disturbed strata and landsliding (e.g. landslide-prone coastal cliffs where currently active bocannes are situated) (Fig. 2.15), indicating that disruption, rapid exposure, and access to atmospheric oxygen are required to produce combustion. Here, the mudstones contain between 1 and 8% carbon consisting of fine detrital vitrinite (humic matter) with a reflectance of 0.25% corresponding to the coal rank of lignite, probable alginite

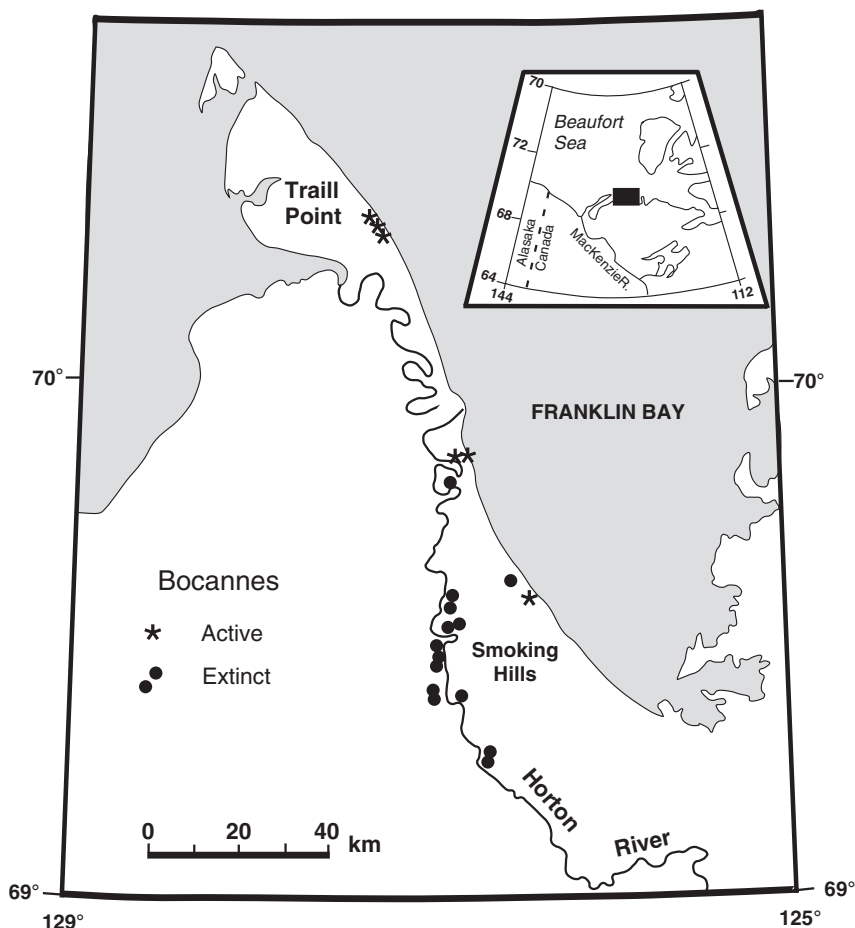


Fig. 2.15 Map of the Smoking Hills area, Canadian Arctic coast, showing the distribution of active and extinct *bocannes* (redrawn from Fig. 1 of Matthews and Bustin 1984). See text in Chap. 3

(sapropelic matter) and pyrite (between ~4 and 30%), in part as minute flamboidal aggregates. Calculated calorific values (kJ/kg^{-1}) range from 360 to 2430 for carbon and from 740 to 2100 for pyrite, and measured total unweathered mudstone calorific values range from 1200 to nearly 4000 kJ/kg^{-1} . Compared to the heat capacity of a typical shale of $0.7\text{--}1.025 \text{ kJ/kg}^{-1}\text{C}^{-1}$ (Handbook of Chemistry and Physics 1979), this is enough energy, given complete combustion at 100% efficiency, to raise the temperature of the mudstone by several thousand degrees. Exothermic peaks for the devolatilisation of combustible gases occur between 280 and 480°C and if these gases were ignited at their point of emergence into the atmosphere they would be able to heat a small volume of the surrounding rock to melting point.

Pyrometamorphism of sediments by burning gas jets is also recorded from Iraq and Iran. In the Injana area of Iraq, burnt and melted rocks make up a line of remnant

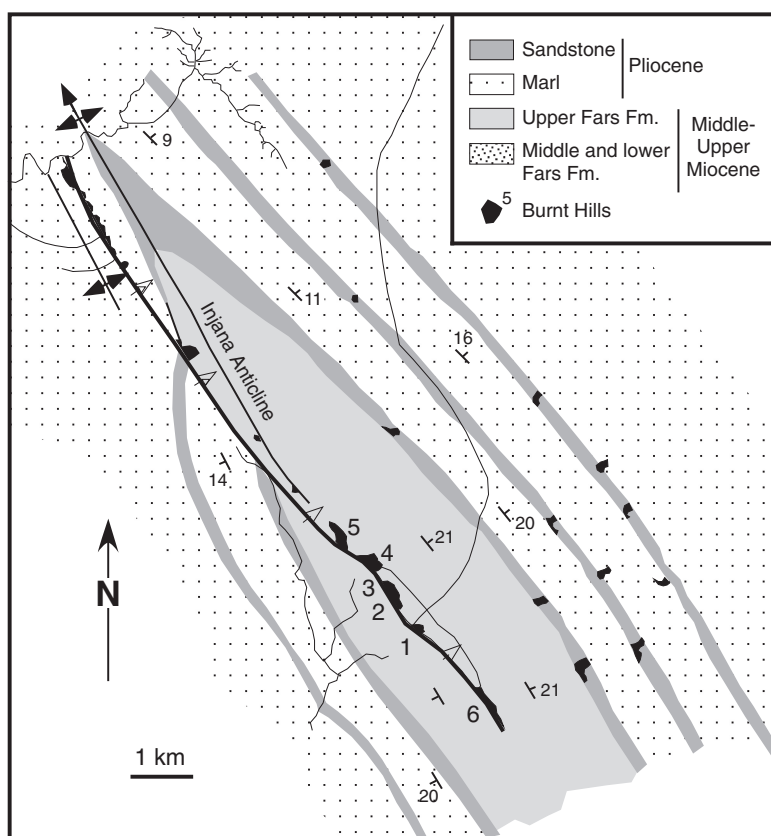


Fig. 2.16 Geological map of the Injana area, Iraq, showing structural setting of “burnt hills” (labeled 1–6) that indicate sites of combustion metamorphism (redrawn from Fig. 1 of Basi and Jassim 1974). See text in Chap. 4

hills situated along a major thrust associated with an anticlinal structure (Fig. 2.16). The hills rise 6–14 m from the surrounding plain and are capped by vesicular and completely crystalline rock that is commonly brecciated. The fused cap rocks are in abrupt contact with underlying baked and partly crystalline grey, yellowish to red marls that grade into unaltered rocks at the base of the hills. The sequence can be interpreted as having formed by the action of burning gas seepages along the thrust fault and the hard, fused nature of the rocks means that they remain as erosion remnants.

Similar baked and fused rocks that occur as conical hills are developed along an anticlinal axis near the head of the Persian Gulf, Iran (McLintock 1932). The distribution of fused and brecciated rocks implies a vent-like structure originating from the explosive escape of gas and oil that became ignited. In this respect, McIntock

(1932) records an instance of the formation of a mud volcano in Trinidad that was accompanied by violent eruption of enormous quantities of inflammable gas. This became ignited by sparks from the abrasion of pyrite fragments to produce a ~90 m high flame that burned for 15 h.

2.3 Lightning Pyrometamorphism

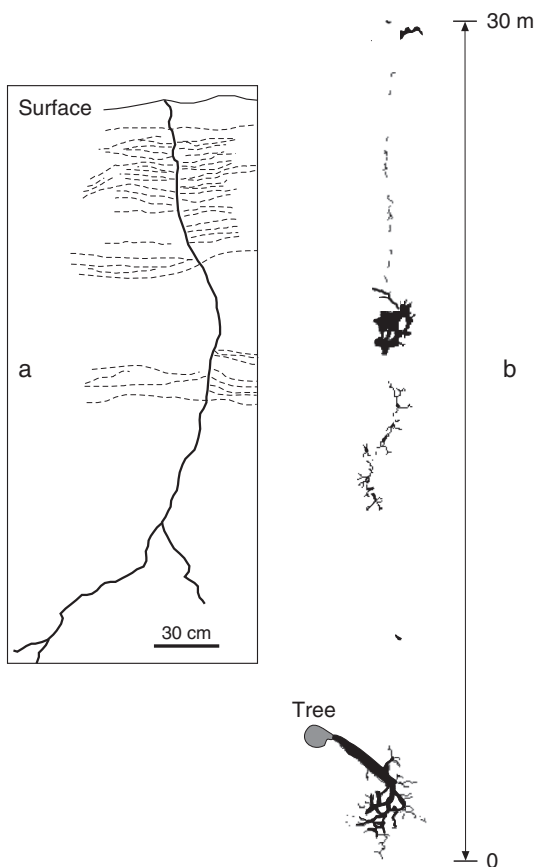
Fulgurites, caused by lightning-induced melting and chemical reduction, provide the thermal limit of pyrometamorphism where temperature maxima are shorter and more extreme by several orders of magnitude than igneous or organic fire-related processes. A lightning bolt is typically about 2–5 cm diameter and attains a speed of 94000 km/s. Times of lightning-induced melting are on the order of a second. Although the pressure remains near atmospheric, temperatures are typically in excess of 2000 K. Voltages (and thus EMF's and chemical potential gradients) are extreme, with peak currents measuring 10 kA and up to 200 kA reached in microseconds (Rakov and Uman 2003, Uman 1969). Therefore, when surface material (sediment or rock) is struck by lightning it undergoes a rapid physical, chemical and morphological change.

Each lightning discharge follows the path of least resistance. This may be single or branching, and is controlled by changes in composition, moisture, compaction and bedding attitude. The tubular form of fulgurites has been attributed by Petty (1936) as the result of expansion of moisture present in impacted sand or soil, expansion of air along the path of the electrical discharge, or from the mechanical displacement of sand which is then fused around the resulting hole. Because many fulgurites form in dry sand, expansion of air is probably the main factor of their formation. The amount of sand that is melted to form the tube will depend on the intensity of the discharge which, in turn, controls the energy expended in the form of heat. The melted sand acquires a cylindrical shape as a result of surface tension, the diameter of which is dependent on the amount of expansion of air and moisture along the discharge path. If the air/moisture expansion is large in proportion to the amount of sand melted, a large diameter thin-walled tube is formed.

Fulgurite formation is common on the Earth's surface and there is a voluminous literature detailing occurrences. They typically consist of glass that often exhibits a fluidal texture and is seldom devitrified. Mostly, fulgurites are quite small with internal diameters in the mm to cm range. The longest fulgurites occur in unconsolidated material such as sand and soil and the longest and deepest-penetrating fulgurite recorded is a little over 4.9 m in length occurring in sandy soil, northern Florida (Fig. 2.17a) where there is an average of 10–15 lightning strikes/km²/year (Wright 1999). In such cases, the bottom limit of fulgurite formation is determined by the ground water table or a layer of wet sediment. As the tubes extend downward from the surface they decrease in diameter and become branched. Pebbles in the path of the discharge cause deflections. Outward projections of thread-like fused silica (lechatelierite) occur over short sections, especially in quartz-rich sand. Terminations of fulgurites vary from glassy, bulbous-like enlargements to an

Fig. 2.17 (a) Sketch from a photograph (redrawn from Fig. 4 of Wright 1999) of a ~2.9 m long fulgurite (*solid black lines*) formed in cross-bedded sands (bedding shown by *sub-horizontal dashed lines*), Florida, USA, where examples over 4.9 m in length have also been found.

(b) The Winans Lake fulgurite (*black*) formed along a morainal ridge in southeastern Michigan, USA. Fulgurite development is concentrated in three separate loci with continuity between the loci indicated by charred soil and vegetation (redrawn from Fig. 1 of Essene and Fisher 1986). See text in Chap. 3



aggregate of loosely cemented partially fused sand grains. Turbulent flow structures may be present in the fulgurite glass and the presence of gaseous bubbles indicates that boiling and vaporisation are associated with the melting process. In other cases, the fulgurite may extend along the ground surface, as shown by the 30 m-long Winans Lake fulgurite, southeastern Michigan, USA (Essene and Fisher 1986) (Fig. 2.17b), which is probably the longest, laterally-extending fulgurite recorded.

While fulgurite formation in sand (*sand fulgurites*) is the most common type reported, *clay-soil fulgurites* are described from the Eastern Goldfields of Western Australia by Gifford (1999). These are different from lightning strikes in sand in that they cause notable disturbance of the clay-rich soil such as that illustrated in Fig. 2.18. The point at which lightning entered the ground is indicated by a 50 cm diameter hole where the ground surface is considerably disturbed with clods of earth being thrown out onto the surface including a piece of vesicular fulgurite presumed to have been thrown into the air at the time of the strike and dropped back on top of the disturbed soil. The ground surface around the point of the lightning strike forms a low conical mound about 6 m in diameter that collapsed when walked on.

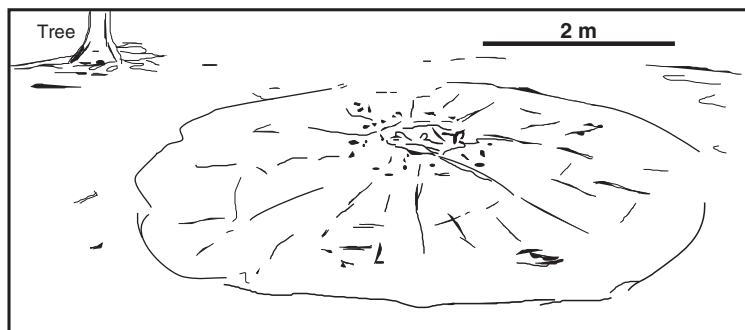


Fig. 2.18 Structure resulting from a lightning strike in clay soil at Avoca Downs, Eastern Goldfields of Western Australia (redrawn from Fig. 1 of Gifford 1999). The sub-surface soil has been expanded to a maximum of ~50 mm at the centre of the strike

It appears that the energy discharge of the strike was dispersed due to the electrical current spreading out radially from the point of impact. The fulgurite formed was small and consisted of a glassy vesicular core surrounded by baked clay which also had a vesicular structure. The nature and pattern of ground disturbance suggest that the path taken by the lightning discharge was controlled by moisture content of the clay soil. The most likely interpretation is that the lightning strike occurred after rain following an extended period of dry weather so that the soil at depth was dry with a shallow damp surface. This allowed the electrical discharge to radiate out from the point of impact within the shallow and more conductive damp surface layer of the soil. The discharge caused considerable heating resulting in the formation of steam and heated gases within the soil that expanded and created the low conical structure. Also, the radial dispersion of the electrical current reduced the development of glass and zoned structure in the fulgurite that formed. An interesting example of another soil fulgurite is where lightning was conducted to the ground via an electric pylon at Torre de Moncorvo, Portugal. The fulgurite consists of a vertical central cylinder that narrows downwards from which radially distributed, essentially horizontal bifurcating branches occur that become smaller in diameter away from the central vertical tube (Fig. 2.19; Crespo et al. 2009). The horizontal radially-branching structures represent dispersion of a large part of the lightning energy within an area of more porous and moist soil near the surface.

In rocks, particularly crystalline ones, the effects are different from sand or clay-soil fulgurites. In this case, fulgurites take the form of glass-lined holes drilled into and sometimes through corners of the exposed rock or produce glass-lined grooves in the rock surface (Fig. 2.20). Millimeter-sized globules of melt may be ejected from these excavations (e.g. Clochiatti 1990, Frenzel and Stähle 1984). The fulgurites so formed often have a zonal structure on a mm scale, with the inner zone being iron-rich (Frenzel et al. 1989). In other cases, the path of the discharge is shown by a black filigrane network, melt threads or films along and over exposed grain boundaries, particularly quartz (e.g. Wimmenauer and Wilmanns 2004) (Fig. 2.21).

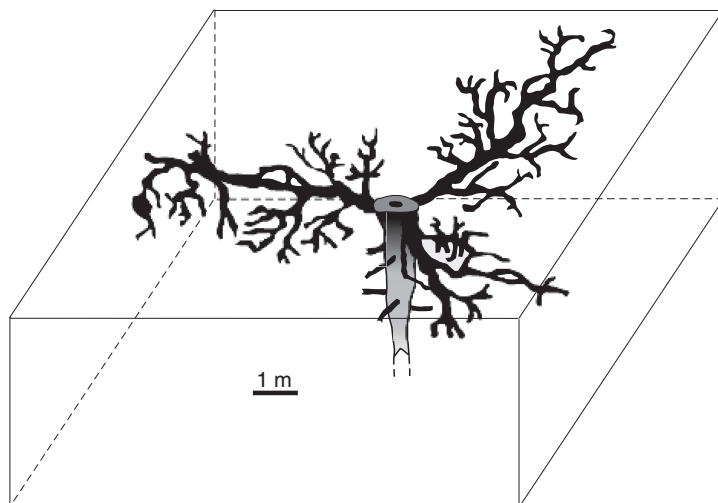
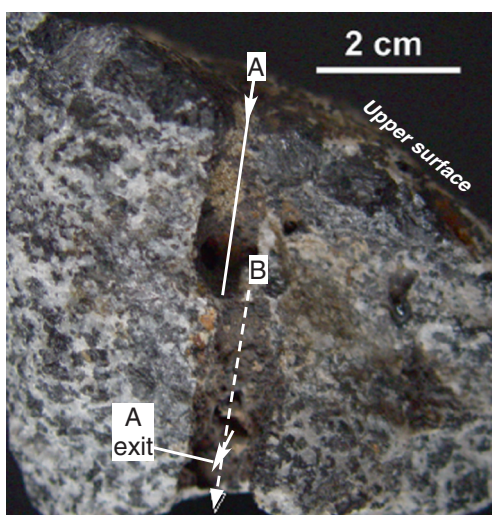


Fig. 2.19 Diagram of a branching fulgurite formed in soil at Torre de Moncorvo, Portugal (redrawn from Fig. 3 of Crespo et al. 2009). See text in Chap. 6

Fig. 2.20 Lightning strike fulgurites in gabbro, Adamello, Cornone di Blumone, Italy, that occur as (A) a glass-lined hole through and exiting the rock and (B) a glass-lined groove excavated in the surface of the rock. See text in Chap. 5



Fulgurite glasses are often compositionally inhomogeneous. In general, reduction occurs during lightning strike melting of rocks and sediment by release of excess oxygen in the vapour, as indicated by the presence of metallic globules (Essene and Fisher 1986, Pasek and Block 2009), but the degree of reduction can vary significantly within a single fulgurite glass (e.g. Sheffer et al. 2006). Variations in mineralogy and composition of the target material will affect the extent of reduction

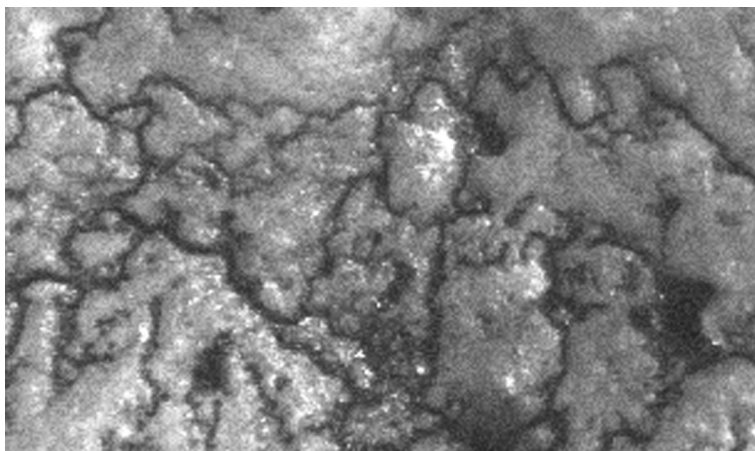


Fig. 2.21 Example of a fulgurite network pattern developed on an exposed quartz surface in granitic rock, Black Forest, Germany (Fig. 12 of Wimmenauer and Wilmanns 2004). Width of photo is 2.7 mm

by lightning strikes. In areas that experience the highest temperatures, e.g. the centre of fulgurite tubes, glass is essentially homogeneous and towards the tube edges it is less homogeneous (less well mixed) on a micron scale and may contain partially fused and unmelted mineral grains, e.g. Switzer and Melson (1972), Frenzel and Stähle (1984). Fulgurite liquids cool isentropically and rapidly quench maintaining high temperature equilibrium pertaining to each micrometer-scale compositional domain that has been melted with vapour being released into the atmosphere.

2.4 Other Thermal Effects

2.4.1 Columnar Jointing

Perhaps the first description of columnar jointing in sandstones was made by Glen (1873) on the Island of Butte, Scotland. He considered that the columnar structure was caused by steam, “or some other highly heated vapour passing upward through a vertical fissure and affecting the sandstone for a few metres on either side”; “The columns are all nearly vertical, none being more than 20° from the perpendicular. Their size varies from six or seven inches [15.2–17.8 cm] in diameter down to half-an-inch [1.3 cm]. Some of the large columns break into smaller ones from exposure to the weather, and others branch into two, forming twin columns. The number of sides varies from four to eight or ten, six being the most common”, e.g. such as that shown in Fig. 2.22.

Mohl (1873) provides a detailed description of columnar jointed sandstone in contact with basalt from localities in Germany.

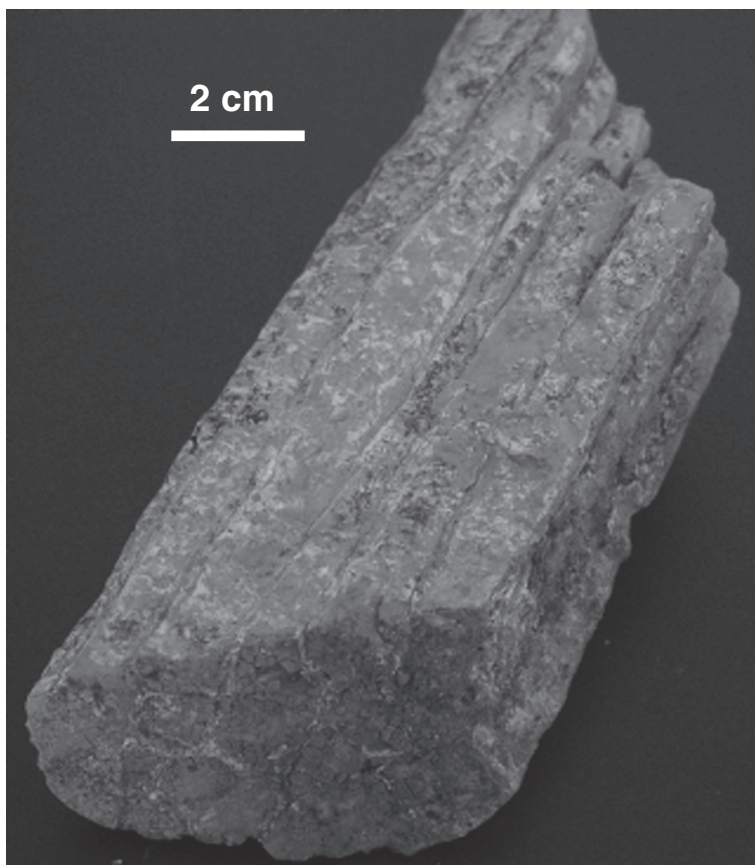


Fig. 2.22 Columnar jointed claystone occurring below a thick basalt flow, Egerli Dag, Iscehisar Province, Turkey (sample supplied by Jörg Keller)

The burned sandstones – long known from the Otzberg – are found in cubic meter sized blocks that are broken into 3 to 8 cm large and 4-, 5- or many fold squared prisms. . . close to the surface some blocs are found which fall apart into quite sharp-edged small columns. Blocks of a white to whitish yellow sandstone which are very soft immediately after being brought above ground, harden in the air. These blocks are usually covered with a dark, chocolate-brown substance several centimetres thick. This material has a curved fractured surface, a nearly waxy lustre, is soft ($H = 2$) with a greasy touch, falls apart immediately with a cracking sound when immersed in water, becomes hard with transparent edges when heated, and melts on coal to a vesicular greenish-brown yellow enamel. Microscopically, the grains that fall out of the substance when put into water as well as fragments of the fused material cannot but be interpreted as light bottle-green relics of augite full of tiny magnetite crystals. The rather imperceptible transition from this substance into a slaty friable, brittle basalt is in favour of interpreting the surrounding substance as a bole-like decomposition product of the basalt. Apart from the jointing no other changes of the sandstone are obvious. The sandstone consists of an argillaceous-carbonaceous cement and contains abundant quartz pebbles.

Sandstone blocks in the basalt separate easily from it . . . the single small columns exhibit an extremely thin, whitish rim with a waxy lustre. This rim does not effervesce when treated with hydrochloric acid but detaches easily as thin films which consist of an aggregate of 0.008 mm diameter, six-sided, faintly polarising, tiny scales of tridymite within an opal-like substance. The sandstone is very tenacious and on cleavage planes partly still sandstone-like and spotted with small humps, partly pervaded by varnish-like shining dark veins, partly completely homogeneously aphanitic and black similar to the basalt itself, but always contains white to greyish, up to 1.5 cm diameter quartz pebbles.

. . . One of the best examples of contact effects is displayed at Stoppelberg near Hünfeld. Here, there is a basalt quarry in the base of which ca. 1m of red sandstone is exposed overlain by basalt. Vertical columns in the basalt, somewhat finer and porous/vesicular towards the base (at the contact), are intimately welded with the sandstone. In the sandstone, columnar jointing continues below the level of the quarry and from the overlying basalt downwards a gradual transition is observable from buchite to more or less sintered sandstone and horizontally-bedded sandstone.

Columnar jointing in coarse-grained arkosic sandstone is also reported by Poddar (1952) cropping out over an area of about 93 m² near Bhuj, northern India. In this case the columns are polygonal, have a thickness of ~8–20 cm and a length of 0.3–0.6 m. Although Poddar considered them to have resulted from contraction after dehydration due to being heated by basaltic dykes, they are in fact, related to combustion of coal seams. Prismatic columnar jointing caused by combustion of organic matter also occurs in bituminous marly rocks of the Mottled Zone, Hatrurim basin, Israel (see Chap. 4) (Avnimelech 1964). The columns are several centimeters in length, contain high temperature minerals such as spurrite, and are interpreted as a cooling-contraction phenomena with the long axes of the columns indicating the direction of the highest thermal gradient (Burg et al. 1992).

The mechanism of producing columnar jointing in partially melted sediment (buchite) adjacent an intrusion is described in detail by Solomon and Spry (1964) in relation to the inclined dolerite pipe at Apsley, Tasmania (Fig. 2.23a). Although the buchite columns plunge at shallow angles and tend to be radial to a small area around the centre of the plug, there is a general departure from the expected condition that they be normal to the igneous contact and there is also local irregularity (Fig. 2.23b). This is probably related to the form of the plug and associated pattern of heat-flow combined with variations in the physical properties (particularly permeability) of the sedimentary layers. The columnar buchites at Apsley contain >40% glass (maximum of ~65%) and plunge mainly at low angles in various directions, although the plunge is constant for each bed but differ from bed to bed. The columns are generally hexagonal with curved faces, but pentagonal, quadrilateral forms also occur.

At a maximum melting temperature of the sediments of around 1000°C at 50 bars PH_2O , the occurrence of buchites up to 140 ft from the southern contact of the dolerite and within a few feet on its NE side, indicates a highly asymmetric heat flow regime suggestive of upward and outward transport of heat by steam (convection rather than conduction) in relation to a steep southward dip of the plug. Under convective conditions, heat-flow would be partly up the buchite zone but largely outward along the sedimentary layers giving rise to the mainly subhorizontal columns

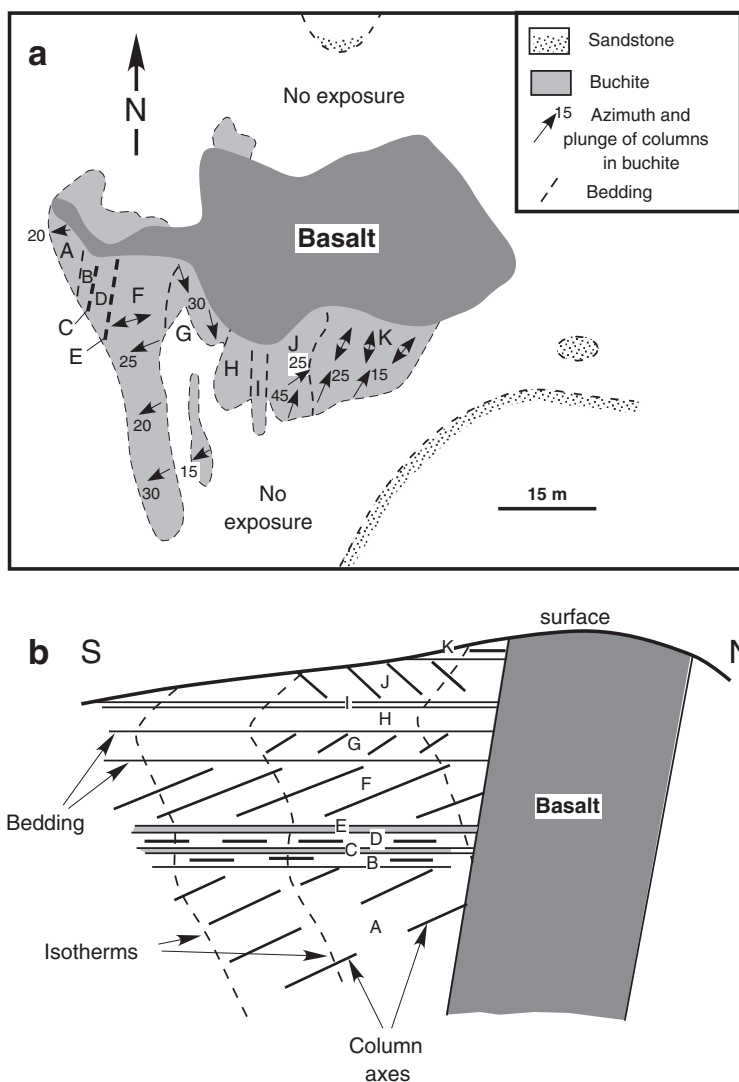


Fig. 2.23 (a) Geological map of the dolerite plug and distribution of columnar buchite at Apsley, Tasmania (redrawn from Fig. 2 of Spry and Solomon 1964). Letters A–K refer to rock-types in sandstone sequence shown in (b) and in Fig. 2.24. (b) Cross section of the dolerite-buchite association at Apsley, Tasmania, showing inferred buchite column orientation under convection conditions as discussed in text (redrawn from Fig. 8b of Spry and Solomon 1964)

observed. This would also explain the irregular distribution of the columnar buchites with gas-phase H_2O penetrating further along those beds with higher permeability resulting in an irregular isotherm pattern within an estimated mass of sandstone converted to buchite of 3×10^{11} g.

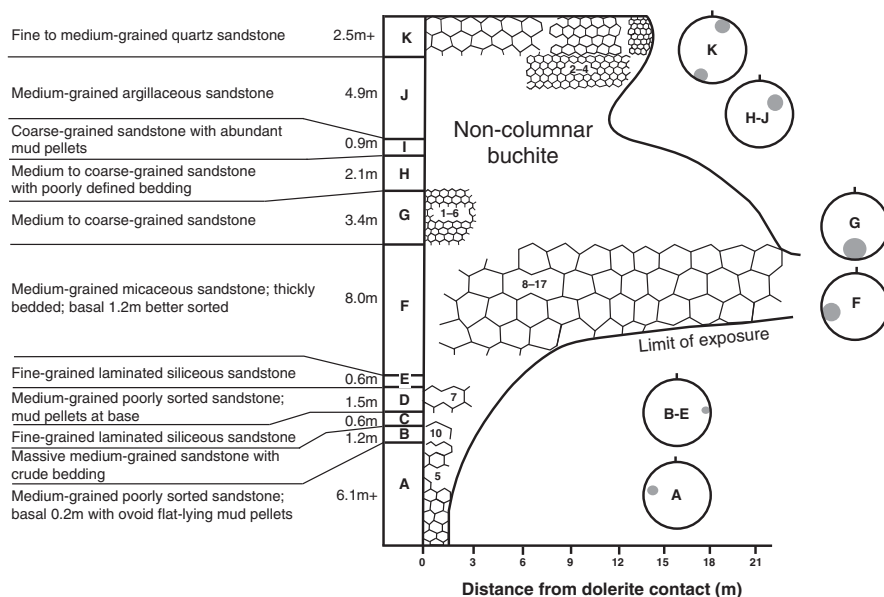


Fig. 2.24 Schematic diagram showing relations between sedimentary succession and distribution, size (diameter range in cm), and attitude (stereographic projections on a horizontal plane of column-axes) of buchite columns associated with the dolerite plug at Apsley, Tasmania (redrawn from Fig. 13a, b of Spry and Solomon 1964)

The columns range in diameter from 2.5–50 cm and are clearly related to lithological variation in the sediments (Fig. 2.24). Primary differences in the type of quartz packing, the composition of other components and their relative proportions and degree of heterogeneity are important factors controlling the shrinkage behaviour of the rocks. Furthermore, unlike the development of columnar structures in igneous rocks, in metamorphosed sedimentary rocks columnar jointing is related to heating as well as cooling. During heating, contraction stresses may be established that can facilitate/accentuate the development of columnar jointing during cooling of the rocks below their softening point, i.e. numerically about half the melting point. Variable degrees of contraction during heating takes place by:

1. Mineral (e.g. clay, mica, chlorite) dehydration resulting in the development of allotropic forms. The proportion of phyllosilicates (mainly clays) is <15% in the Apsley sediments and the effects of phyllosilicate contraction would be countered by the greater percentage of quartz that expands on heating.
2. Reaction to anhydrous minerals with greater density, e.g. muscovite, chlorite reacting to spinel, mullite, corundum, etc.
3. Structural adjustment due to recrystallisation and consequent reduction in pore space, e.g. the change of sandstone to quartzite results in an increase in specific gravity from 2.2 (sandstone) to 2.6 (quartzite) and a shrinkage of 18%.

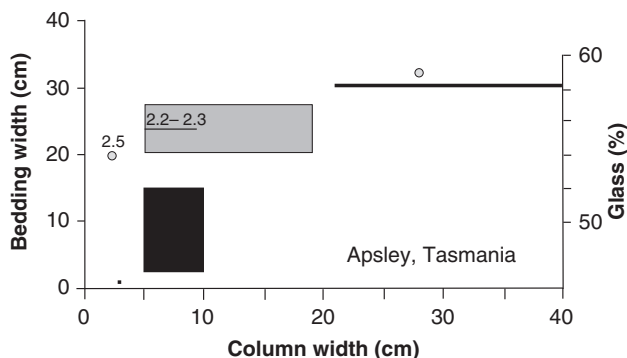


Fig. 2.25 Plot of bedding width versus buchite column width and vol.% glass versus buchite column width, Apsley, Tasmania (data from Spry and Solomon 1964). See text

4. Formation of melt which allows repacking and fills pore-spaces. This is probably the main cause of shrinkage. The increase in specific gravity from ~2.1–2.2 in sandstone to 2.2–2.4 in buchites with increasing glass (Fig. 2.25) indicates a decrease in volume amounting to a shrinkage of 5–10%.

Larger columns occur in more massive, thickly bedded sandstones. They also contain more glass (Fig. 2.25), and hence have a greater tensile strength resulting in more widely spaced fractures. The more glass in a buchite, the less it will contract and fracture for a given temperature change. The smallest columns of ~2.5 cm occur in thinly-bedded sandstone (Fig. 2.24) and they do not form in beds that contain abundant mud pellets or in siltstones (porcellanites). It is probable that the mud pellets introduced sufficient irregularity in the tensile stress-pattern developed by shrinkage that columnar joints could not form. The original shaley nature of the porcellanites and possibly also closely spaced partings, modified the stress-pattern and fracture-growth inhibiting the development of columns.

2.4.2 Microcracking

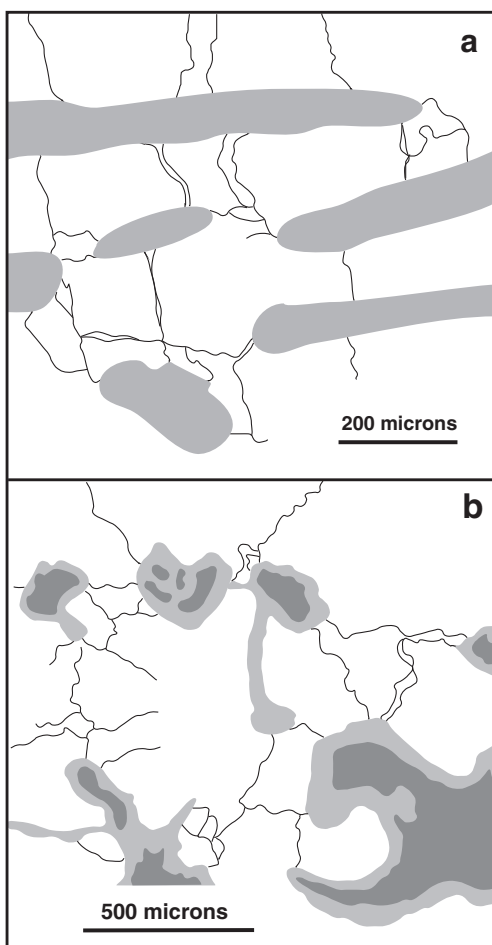
Because melting reactions generally involve a positive volume increase at the melting site, rapid melting causes the development of high melt pressures leading to hydraulic fracturing and migration of melt along these fractures. Several generations of such microfractures in gneissic psammitic and pelitic rocks within 3.5 m of a 6 m thick basic sill are described by Holness and Watt ((2001). Up temperature (>600°C) crack development is caused by the breakdown of muscovite and melting along quartz-feldspar boundaries. The earliest generation of microcracks related to the pyrometamorphic event cut across quartz and feldspar crystals but rarely across their respective boundaries and are thought to be the result of anisotropic thermal expansion associated with a contribution from the α – β inversion in quartz which occurs at ~590°C at 600 bars.

A second generation of cracking involving the formation of two sets of microcracks relates to the breakdown of muscovite according to the fluid-absent reaction



This metastable reaction involves an increase in volume of perhaps ~5–7% that causes overpressuring and grain-scale fracturing (Brearley 1986, Connolly et al. 1997, Rushmer 2001). In the example described, the microcracks radiate away from muscovite grains and are melt-filled (Fig. 2.26). They also appear to re-use cracks that existed in the rocks prior to the pyrometamorphic event. No obvious microcracking is associated with the fluid-absent, metastable breakdown of biotite, possibly because this involves a much smaller positive volume change (Rushmer 2001).

Fig. 2.26 Diagrams showing microcracking during pyrometamorphism of sediments in contact with the Traigh Bhàn na Sgùrra sill, Isle of Mull, Scotland (see text). **(a)** Psammite, 80 cm from the contact showing microcracks extending from muscovite grains (*grey*) partly reacted around margins to cordierite, into quartz (*white*). Cracks have developed at a high angle to the foliation indicated by alignment of muscovite (redrawn from a CL image Fig. 9 of Holness and Watt 2001); **(b)** Psammite, 44 cm from the contact showing a largely interconnected pattern of cracks that are melt-filled and extend outwards along boundaries of quartz grains (*white*) from crystallised (granophyric) rims (*light-grey shading*) that surround partly melted feldspar (*dark-grey shading*) (redrawn from CL image Fig. 13d of Holness and Watt 2001)



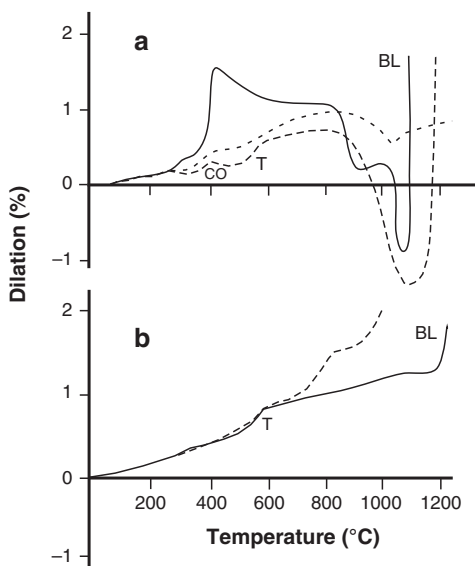
The penultimate stage of microcracking occurs with melting at quartz-feldspar grain boundaries. Cracks form along the grain boundaries and extend into the grains and outwards across adjacent grains (Fig. 2.26). They are extremely common within 80 cm of the sill contact where temperatures were higher than 900°C. Despite the high degree of melt-filled fracture connectivity, there is little evidence of melt segregation presumably because of the static nature of the pyrometamorphic event. The last stage of cracking occurred during cooling and produced cracks that cut across or reopen solidified melt-filled fractures. In addition to anisotropic thermal contraction of the rock, these cracks could have been produced by a reversal of the α - β quartz inversion at 575°C.

2.4.3 Dilation

Heating at atmospheric pressure due to combustion of coal seams often results in dilation of sediments overlying the burning coal seam. Cavities may remain open and provide space for vapour phase crystallization of high (sanidine facies) and low temperature (hydrous) minerals or become filled by melt. Heating experiments conducted by Wolf et al. (1987) on siltstone and shale that overlie coal seams in Belgium indicate the effects of devolatilisation, decarbonation and vitrification on rock dilation between 100 and 1200°C related to combustion of the coal. The experiments were conducted at 25 bars with a heating rate of 0.5°C/min and the results are shown in Fig. 2.27.

In *clay-rich* siltstone (Fig. 2.27a), dilation is moderate but constant with increasing temperature except for an increase at the α - β quartz inversion at 587°C.

Fig. 2.27 Dilation curves (warming-up rate of 0.5°C/min) for: (a) Shale with dispersed organic matter (*solid line*); Shale with dispersed organic matter and with silt and coal streaks parallel to the cleavage (*thin dashed line*); Shale with dispersed organic matter and with silt and coal streaks normal to the cleavage (*thick dashed line*) (redrawn from Fig. 2 of Wolf et al. 1987); (b) Siltstone with carbonate matrix (*dashed line*); siltstone with clay matrix (*solid line*) (redrawn from Fig. 1 of Wolf et al. 1987). CO = coking; T = transition from α - β quartz; BL = bloating



Vitrification at $\sim 900^\circ\text{C}$ does not change the dilation pattern; surfaces of the heated samples become glassy and degasification channels and vesicles form. Bloating occurs at $\sim 1200^\circ\text{C}$ resulting in a marked increase in dilation. In siltstone with a *carbonate-matrix*, decomposition of dolomite and siderite results in a marked dilation due to bloating between 600 and 900°C .

In comparison with siltstones, carbonaceous shale exhibits much more dilatatory variation (Fig. 2.27b). Between 100 and 200°C , fracturing parallel to cleavage occurs in response to dehydration and dehydroxylation of clay minerals. From $\sim 390^\circ\text{C}$, coking of organic matter causes an increase in dilation, particularly where the organic material is dispersed rather than occurring as coal streaks. Formation of melt above $\sim 850^\circ\text{C}$ results in shrinkage that continues up to $\sim 1050^\circ\text{C}$ and is reversed above $1050\text{--}1100^\circ\text{C}$ when bloating associated with vesiculation occurs. Wyllie and Tuttle (1961) also report that half-melted shales in their melting experiments are extremely vesicular and have a frothy, slaggy appearance.

2.4.4 Preservation of Glass and Glass Compositions

The terms *buchite* and *paralava* imply the presence of glass (quenched melt). While quenching would occur in partially fused xenoliths on eruption, this is not the case for slower cooled wall rocks at the contacts of sills, dykes and plugs and for xenoliths that they contain. Because rocks are poor conductors of heat, rapid cooling of melts does not seem possible in these circumstances and so the question of why glass often remains largely undevitrified in many pyrometamorphic rocks needs explanation.

Figure 2.28 shows that above the “glass transformation temperature” (T_g), a temperature dependent on cooling rate over which melt becomes solid (glass) and hence a temperature range, a supercooled liquid is stable. Below T_g , glass is stable. A melt cooled to the vicinity of the T_g region will rapidly devitrify to a crystalline aggregate. If cooling is very rapid (as in quenching) only glass forms. At progressively slower cooling rates more and more crystal nuclei are able to form as the melt passes through the T_g range. If sufficiently rapid, only a few crystal nuclei will form and the end product will be largely glass containing a few crystals. Glass will crystallise only if held for a certain time above T_g , i.e. the temperature at which viscosity is probably in the order of 10^{13} Pa’s. At this viscosity, glasses devitrify rapidly, i.e. in $10\text{--}10^3$ s. At a higher viscosity, e.g. 10^{14} Pa’s, glass could be expected to devitrify in $10^2\text{--}10^4$ s. Liquids produced by melting of sediments are essentially alkaline aluminosilicates and would have high viscosity. If this were 10^{16} Pa’s, then it would not crystallise if cooled from a high temperature over several months and would remain glass provided it was not subjected to the influx of water (e.g. Spry and Solomon 1964). Once formed, the preservation of glass in a contact aureole will also depend on whether fluid infiltration occurs during cooling.

An instructive case is the glass-rich quartzose metasediments that occur within 0.8 m of the Glenmore dolerite plug, Ardnamurchan, Scotland (Butler 1961,

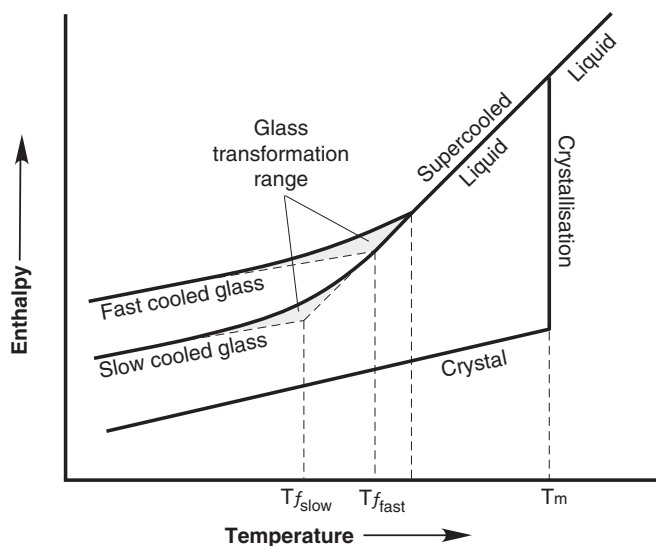


Fig. 2.28 Diagram illustrating the effect of temperature on the enthalpy (or volume) of a glass-forming melt (redrawn from Fig. 1.1 of Shelby 1997). See text

Holness et al. 2005). Given that metamorphism occurred at a depth of several hundred meters (~120 bars), it seems unlikely that the presence of glass was caused by rapid cooling but rather to the absence of pervasive fluid infiltration which would be expected to have caused extensive devitrification to a micrographic (granophytic)

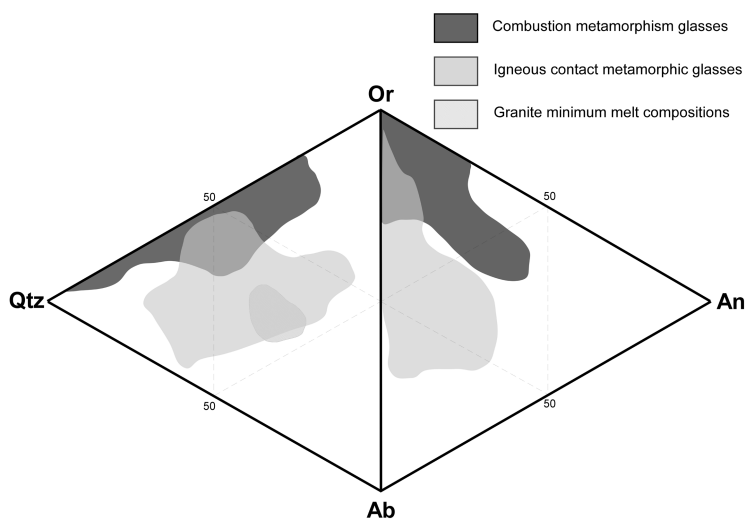


Fig. 2.29 Normative Qtz-Or-Ab and Qtz-Ab-An composition fields of glasses in buchites of igneous pyrometamorphism and paralava-clinker of combustion pyrometamorphism

texture of quartz and feldspars. At Glenmore, late-stage hydrothermal fluid circulation was channeled through vein systems. Cooling rate was also important. In the relatively slowly cooled outer part of the aureole (see Fig. 2.1), the melt crystallised. In the transition zone to the inner aureole only the quartz component of the melt crystallised, while in the relatively rapidly cooled inner aureole, i.e. within 0.2 m of the contact, all the melt solidified to glass. On the basis of a thermal model developed by Holness et al. (2005) that ignores possible effects from latent heat of crystallization (see Chap. 3), the critical cooling rate for glass formation is estimated to have been ca. $8^{\circ}\text{C}/\text{day}$.

Glass compositions in buchites and paralavas described in the following chapters are plotted in Fig. 2.29 in terms of normative quartz (Qtz), albite (Ab), orthoclase (Or) and anorthite (An) components that typically form $> 90\%$ of their compositions. In these pyrometamorphic rocks, especially paralavas, the glass is a residual phase in that it represents the quenched melt from which high temperature phases have crystallized. Such glasses tend to be Or- and Qtz-rich. In the early stages of fusion, such as between quartz, feldspars and muscovite, as seen in some buchites, many of the lower temperature normative glass compositions are similar to granitic minimum melts as shown in Fig. 2.29.



<http://www.springer.com/978-3-642-15587-1>

Pyrometamorphism

Grapes, R.

2010, XI, 365 p., Hardcover

ISBN: 978-3-642-15587-1